J Biomol NMR (2015) 63:97–109
DOI 10.1007/s10858-015-9972-1

ARTICLE

Dynamic nuclear polarization of nucleic acid with endogenously bound manganese

Patricia Wenk[1,3] · Monu Kaushik[1] · Diane Richter[1] · Marc Vogel[2] · Beatrix Suess[2] · Björn Corzilius[1]

Received: 12 May 2015 / Accepted: 22 July 2015 / Published online: 29 July 2015
© Springer Science+Business Media Dordrecht 2015

Abstract We report the direct dynamic nuclear polarization (DNP) of ^{13}C nuclei of a uniformly [^{13}C,^{15}N]-labeled, paramagnetic full-length hammerhead ribozyme (HHRz) complex with Mn^{2+} where the enhanced polarization is fully provided by the endogenously bound metal ion and no exogenous polarizing agent is added. A ^{13}C enhancement factor of $\varepsilon = 8$ was observed by intra-complex DNP at 9.4 T. In contrast, "conventional" indirect and direct DNP experiments were performed using AMUPol as polarizing agent where we obtained a ^{1}H enhancement factor of $\varepsilon \approx 250$. Comparison with the diamagnetic (Mg^{2+}) HHRz complex shows that the presence of Mn^{2+} only marginally influences the (DNP-enhanced) NMR properties of the RNA. Furthermore two-dimensional correlation spectra (^{15}N–^{13}C and ^{13}C–^{13}C) reveal structural inhomogeneity in the frozen, amorphous state indicating the coexistence of several conformational states. These demonstrations of intra-complex DNP using an endogenous metal ion as well as DNP-enhanced MAS NMR of RNA in general yield important information for the development of new methods in structural biology.

Keywords Dynamic nuclear polarization (DNP) · Solid-state NMR · EPR · RNA · Transition metal · Polarizing agent

Introduction

Solid-state magic-angle spinning (MAS) NMR applications to nucleic acid including ribonucleic acid (RNA) are scarce (Abramov and Goldbourt 2014; Cherepanov et al. 2010; Huang et al. 2012; Marchanka et al. 2015), especially when compared to the abundance of solution-state NMR techniques in RNA structural biology (Bothe et al. 2011; Fürtig et al. 2003; Rinnenthal et al. 2011; Sripakdeevong et al. 2014). On the other hand, MAS NMR is invaluable for structural investigations of biomolecules which has been demonstrated in wide-spread applications to protein structural biology (Bayro et al. 2010; Castellani et al. 2002; Wasmer et al. 2008). MAS NMR has advantages over solution NMR when large molecules or molecular complexes are studied since their rotational tumbling is too slow for standard solution NMR. Additionally, the quantitative determination of dipole (through-space) couplings can yield precise internuclear distances. However, short decoherence times as well as incomplete dynamic averaging of local fields often result in intrinsically larger line widths and lower sensitivity.

Because RNA contains only four chemically similar nucleotides—each comprised of a ribose moiety and either a purine (adenine, guanine) or pyrimidine (cytosine, uracil) nucleobase—there is a large potential for spectral overlap of resonances arising from equal or similar

Electronic supplementary material The online version of this article (doi:10.1007/s10858-015-9972-1) contains supplementary material, which is available to authorized users.

✉ Björn Corzilius
corzilius@em.uni-frankfurt.de

[1] Institute of Physical und Theoretical Chemistry, Institute of Biophysical Chemistry und Center for Biomolecular Magnetic Resonance (BMRZ), Goethe University, Max-von-Laue-Str. 7-9, 60438 Frankfurt am Main, Germany

[2] Department of Biology, Technical University Darmstadt, Schnittspahnstraße 10, 64287 Darmstadt, Germany

[3] Present Address: Werner Siemens Imaging Center and Department of Preclinical Imaging and Radiopharmacy, University of Tübingen, Röntgenweg 13, 72076 Tübingen, Germany

nucleobases. Furthermore, resonance assignment based on scalar couplings is complicated because the connecting, generic ribofuranose phosphodiester groups put unique nucleobases at distances of >10 chemical bonds. Here, solid-state NMR has the advantage of generally being able to utilize dipolar (through-space) instead of scalar (through-bond) couplings which allows for direct determination of contacts between nuclei of neighboring nucleobases in the same RNA strand (Marchanka et al. 2015).

Dynamic nuclear polarization (DNP) has been introduced to overcome the MAS NMR sensitivity issue by increasing the intensity of signals by several orders of magnitude (Becerra et al. 1993; Hall et al. 1997; Overhauser 1953). During irradiation with microwaves (mw) of appropriate frequency the large electron spin polarization of a paramagnetic polarizing agent is transferred to surrounding nuclear spins in a frozen solution at cryogenic temperatures of $\sim$100 K. The polarization increase is quantified by the enhancement factor, ε, which is the ratio of the NMR intensity under mw irradiation (mw on), I_{on}, with that under thermal equilibrium conditions (mw off), I_{off}:

$$\varepsilon = \frac{I_{\text{on}}}{I_{\text{off}}} \tag{1}$$

The theoretical maximum is given by the ratio of the electron and nuclear gyromagnetic ratios, γ_S and γ_I, respectively, and reaches 660 for ^{1}H and 2620 for ^{13}C. DNP can be performed indirectly by hyperpolarizing ^{1}H and successively transferring the enhanced nuclear polarization to the nuclear species of interest, or by directly hyperpolarizing the nuclei to be detected (Maly et al. 2010). The former method leads to a uniform enhancement of all proton spins within a few seconds of polarization build-up due to efficient ^{1}H–^{1}H spin diffusion; the latter is often limited by slow diffusion between heteronuclei, especially when nuclei with small abundance are to be polarized (Maly et al. 2010). Nevertheless, slow spin-diffusion can potentially be utilized in order to control the spatial distribution of enhanced polarization.

Most typically, small paramagnetic molecules being dissolved in the cryoprotecting matrix are used as polarizing agents (Hu 2011). Bis-nitroxide biradicals provide for highly efficient cross effect (CE) DNP by evoking a three-spin mechanism within the anisotropic electron paramagnetic resonance (EPR) spectrum under MAS (Hu et al. 2004; Kessenikh et al. 1963). This makes CE the mechanism-of-choice for uniform, indirect DNP (Ni et al. 2013). For intramolecular or intra-complex DNP with endogenous polarizing agents CE is often unfeasible due to the reliance on strong inter-electronic couplings (Hovav et al. 2012; Hu et al. 2011). Therefore, a simpler mechanism—which is easier to analyze quantitatively—is provided by the solid effect (Abragam and Proctor 1958; Corzilius et al. 2012; Hovav et al. 2010; Jeffries 1957, 1960; Smith et al. 2012; Wenckebach 2008). In short, the solid effect (SE) can be selectively evoked for any nucleus by selective irradiation of the electron–nuclear zero or double quantum transition with a microwave frequency of

$$\omega_{\text{mw}} = \omega_{0S} \pm \omega_{0I}, \tag{2}$$

where ω_{0S} and ω_{0I} are the electron and nuclear Larmor frequencies, respectively. This leads to the requirement of paramagnetic species with extremely narrow lines, especially for direct SE of nuclei with small gyromagnetic ratio such as ^{13}C or ^{15}N.

We have shown earlier that—for the SE—a quantitative analysis of DNP efficiency can be performed by careful measurement of the DNP enhancement factor, the build-up time constant of enhanced nuclear polarization, as well as the nuclear longitudinal relaxation time constant without DNP (Corzilius et al. 2012). By knowledge of DNP enhancement and spin relaxation properties direct information about distance may be obtained after calibration with a model system of known electron–nuclear separation. Therefore our study shall serve as an early proof-of-concept for the feasibility of transferring electron spin polarization from an endogenous metal ion to nuclei within the same biomolecule, since such a transfer has never been demonstrated before.

DNP with endogenous radicals in proteins (Maly et al. 2012) as well as nitroxides covalently attached to lipids (Fernández-de-Alba et al. 2015; Smith et al. 2015) or proteins (Wylie et al. 2015) has already been demonstrated to yield moderate ^{1}H enhancement factors of $\sim$10. Nevertheless, fast ^{1}H–^{1}H spin diffusion limits the potential to directly extract structural information by these indirect DNP approaches. We have shown earlier that paramagnetic metal ions like Gd^{3+} or Mn^{2+} can be utilized as polarizing agents which makes them ideal candidates for intra-complex DNP of biomolecules (Corzilius et al. 2011). Mn^{2+} is highly abundant in biological systems or can often readily substitute diamagnetic Mg^{2+}. The central EPR transition ($m_S = -\frac{1}{2} \leftrightarrow +\frac{1}{2}$) of the high-spin ($S = \frac{5}{2}$) system often features narrow lines at high field. This allows for efficient polarization of nuclei with small gyromagnetic ratio such as ^{13}C or ^{15}N using SE. Although in the case of Mn^{2+} the electron spin is strongly hyperfine coupled to the 100 % abundant $I = \frac{5}{2}$ ^{55}Mn nucleus significant ^{13}C enhancement can be achieved as will be shown below.

The biomolecule we utilized as a model system belongs to the well-studied group of hammerhead ribozymes, of which the first construct has been discovered in the late 1980s as a self-cleaving structural element of virusoids and viroids (Forster and Symons 1987; Hutchins et al. 1986;

Prody et al. 1986). It was found early that the self-cleavage reaction strongly depends on the presence of a divalent metal ion as co-factor (Dahm and Uhlenbeck 1991). The structure of a 'minimal' HHRz construct has been solved early under several conditions (Pley et al. 1994; Scott et al. 1995); however, it has been shown later that tertiary contacts between stem loops—missing in the minimal structure—play an important role in ribozyme function (De la Peña et al. 2003; Khvorova et al. 2003). The 'extended' or 'full-length' construct includes those conserved loop regions and the structure was solved by XRD (Martick and Scott 2006). All hammerhead ribozyme (HHRz) varieties share a highly conserved catalytic core region which contains several binding sites for divalent ions such as Mg^{2+} or Mn^{2+} (Scott et al. 1995). Binding of a divalent ion to one of these sites triggers a conformational change and allows for the self-cleavage reaction to occur (Bassi et al. 1996; Murray et al. 1998; Scott et al. 1996). Additional less-specific metal binding sites show a similar affinity towards monovalent ions and are completely saturated under large Na^{+} concentrations ($\geq$1 M) (Horton et al. 1998; Schiemann et al. 2003). The core region is flanked by three stems which give HHRz a robust fold; nevertheless the core region features large internal dynamics. The combination of its moderate molecular size and internal dynamics make the full-length HHRz difficult to access using solution NMR methods—as can be seen when comparing the abundance of NMR studies on the minimal structure (Fürtig et al. 2008; Hammann et al. 2001; Osborne et al. 2009) with the absence of such studies on the full-length variant. Thus it serves as an ideal system for demonstration of DNP-enhanced MAS NMR.

In this study we investigated DNP-enhanced NMR spectroscopy on an inactive 18.0 kDa, 59-mer cis-acting full-length HHRz; the sequence and secondary structure prediction are shown in Fig. 1a and the proposed tertiary fold with loop–loop interactions in subplot b. To inactivate the HHRz the adenosine at position 53 was mutated to a guanosine (Yen et al. 2004). In-vivo functionality of the unmutated construct and effective inactivation due to this point-mutation has been shown in previous studies (Beilstein et al. 2015; Wittmann and Suess 2011). The position of the specific binding site for Mg^{2+} or Mn^{2+} is still heavily debated. In the minimal structure, selective binding of the divalent ion was found in XRD structures predominantly between the phosphate of an adenosine and neighboring guanosine (A36 and G37 in Fig. 1a) within the catalytic core on the opposite site of the cleavage position (between C7 and C8 in Fig. 1a) and the importance of this binding site was confirmed by a functional analysis upon base depletion; catalysis then requires the adaption of a transient conformational state with the divalent ion bridging to the scissile phosphate (Scott et al. 1995; Wang et al. 1999). The nature of

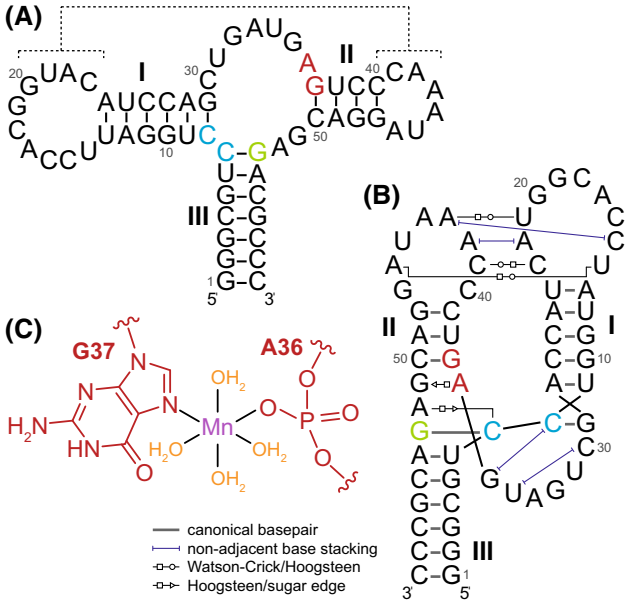

Fig. 1 **a** Predicted secondary structure of the investigated full-length HHRz (inactivated). Canonical base paring interactions are shown with *black lines* within stems. The A-to-G base mutation at position 53 (marked in *green*) is preventing self-cleavage between two cytidines marked in *blue*. The proposed selective binding site for divalent ions is marked in *red*. Tertiary loop–loop interactions are indicated by *dashed lines*. **b** Depiction of the same structure demonstrating possible tertiary interactions between stem-loops II and III as observed in the active construct (Martick and Scott 2006). *Black lines* show sequence continuity. **c** Proposed complex geometry of selective Mn^{2+} binding site (Morrissey et al. 2000; Wang et al. 1999)

the binding site has also been investigated with EPR spectroscopy (Morrissey et al. 1999, 2000). In the case of the extended or full-length HHRz the catalytically active structure is expected to allow for stable closing of the AG active binding site and the scissile phosphate in the cleavage site via a bridging divalent ion (Ward and DeRose 2012). However, in the XRD structure selective binding to only the AG active site has been observed, especially in the case of Mn^{2+} (Martick et al. 2008).

Materials and methods

Nucleic acid preparation

The inactivated full-length hammerhead ribozyme (HHRz) shown in Fig. 1 was transcribed in vitro using the *Sma*I linearized plasmid pHHI as template (the full plasmid sequence is available upon request). The plasmid codes for the T7 promotor followed by the HHRz. The in vitro transcription was carried out in a volume of 10 mL over night at 37 °C with a final concentration of 20 mM magnesium acetate, 0.2 M Tris–HCl (pH 8.0), 20 mM dithiothreitol

(DTT), 2 mM spermidine, 0.2 mg/mL plasmid, 7.5 μg/mL T7 RNA polymerase (purified in the lab) and 4 mM of each nucleoside triphosphate (NTP); for uniformly [^{13}C,^{15}N] isotope labeled HHRz 3 mM of each uniformly ^{13}C,^{15}N-labeled NTP (Silantes) was used. The isotope labeled NTPs were purified by ethanol precipitation and resuspended in purified water prior to transcription. After the transcription the precipitated pyrophosphate was pelleted by centrifugation and EDTA was added to the supernatant to a final concentration of 10 % (v/v). After ethanol precipitation we performed a denaturing polyacrylamide gel electrophoresis (PAGE, 8 % PAA, 8 M urea). The RNA was detected by ultraviolet shadowing, cut out of the gel and eluted from the gel in 0.3 M sodium acetate (pH 6.5) at 4 °C overnight. Afterwards we filtered the supernatant to remove remaining gel slices using a 0.45 μm filter (Sarstedt, Nürnberg, Germany). The RNA was again ethanol precipitated, dissolved in purified water and the concentration was determined via UV/Vis spectroscopy by a ND-1000 spectrophotometer (Thermo Fischer Scientific, Wilmington, DE). A native PAGE assay was used to confirm purity of the RNA (Fig. S1). The HHRz was then lyophilized for storage and further handling.

EPR spectroscopy

For the determination of the Mn–HHRz dissociation constant (K_D) solutions of 62.5 μM HHRz with varying $MnCl_2$ content between 1 μM and 0.2 mM were prepared in triethanolamine (TEA) buffer (40 mM, pH 7.5) with 0.2 M NaCl. In comparison, an additional set of samples was prepared without addition of HHRz in order to demonstrate applicability and linearity of the method. Continuous-wave (cw) EPR was performed using an X-band Bruker EleXsys E500 spectrometer with attached ER 4102ST resonator employing a TE_{102} rectangular cavity. The sample (~10 μL) was contained inside a clear fused quartz (CFQ) capillary with 1.1 mm inner diameter (i.d.) in order to minimize penetration of the sample volume into the electric field region and reduce dielectric losses. Care was taken that each sample tube was positioned equally inside the resonator. Spectra were taken under 10 dB of microwave attenuation (~20 mW power). 100 kHz magnetic field modulation with 1.5 mT amplitude was applied. The field was swept with 82 ms conversion time over 1024 points and signal was integrated with a 41 ms time constant. Each spectrum was accumulated over 20 scans.

The confirmation of Mn^{2+} binding to HHRz in DNP samples was performed directly on the samples used for DNP enhanced NMR spectroscopy as described below. The same instrumentation was used as for K_D determination. Spectra were taken under 20 dB of microwave attenuation (~2 mW power). 100 kHz magnetic field modulation with 0.4 mT amplitude was applied. The field was swept with 164 ms of conversion time over 1024 points and signal was integrated with a 164 ms time constant. Each spectrum was accumulated over 8 scans.

180 GHz EPR spectroscopy was performed using a custom-built spectrometer described elsewhere utilizing a cylindrical TE_{011} cavity resonator (Rohrer et al. 2001). The samples were prepared by dissolving an equal amount of HHRz and $MnCl_2$ in TEA buffer (40 mM triethanolamine, 0.2 M NaCl) and subsequent addition of glycerol, so that a glycerol/water (60/40 vol.%) cryoprotecting mixture with 62.5 μM final Mn–HHRz concentration was achieved. The sample was contained within a 0.4 mm i.d. quartz capillary. Experiments were performed at a temperature of 80 K. Pulse lengths (30 ns for 90° and 45 ns for 180°) and separation (200 ns) of the Hahn echo sequence were optimized for maximum signal intensity and the field-swept spectrum was detected by integrating over the full echo width and averaging over 400 shots with 0.7 ms repetition time in a single scan.

DNP sample preparation

0.9 mg HHRz in lyophilized form was dissolved in 0.2 mL buffer solution containing 40 mM TEA and 0.2 M NaCl. The solution was split in three equal volume samples and lyophilized again. To each sample 40 μL of cryoprotecting solution consisting of 60 % $^{12}C_3$,d_8-glycerol (99.95 % ^{12}C, 98 % D; Euriso-Top), 30 % D_2O (99.9 % D; Sigma-Aldrich), and 10 % H_2O was added, together with an equimolar amount of $MnCl_2$ or $MgCl_2$ with respect to RNA. Final concentrations were 0.4 mM of RNA and $MnCl_2$ or $MgCl_2$, 0.33 M NaCl. For CE DNP 5 mM AMUPol (SATT Sud-Est, Marseille, France) was added. For comparison of build-up dynamics (see Table 1) and as cw EPR reference for unbound Mn^{2+} (see Figs. 6 and S3) 0.4 mM $MnCl_2$ and 225 mM ^{13}C,$^{15}N_2$-urea (99 % ^{13}C, 98 % ^{15}N; CortecNet, Voisins-Le-Bretonneux, France) were dissolved in the $^{12}C_3$,d_8-glycerol/D_2O/H_2O mixture as described above.

DNP-enhanced MAS NMR spectroscopy

For experiments using bis-nitroxide as polarizing agent we utilized a commercially available Bruker AVANCE II DNP spectrometer operating at 400.2 MHz ^{1}H frequency with a Bruker Ultrashield 9.4 T widebore (89 mm) magnet. 263.4 GHz microwaves were produced by a Bruker gyrotron with 60 mA of beam current at which we found an optimum ^{1}H enhancement for AMUPol. Experiments were performed at 112 K (mw on) or 104 K (mw off), read out via a thermocouple inside the MAS stator.

For direct DNP using Mn^{2+} as polarizing agent we utilized a commercially available Bruker AVANCE III DNP

Table 1 ^{13}C enhancement factors and polarization build-up time constants

Sample	T (K)[a]	ε	$T_{B,f}^{(^{13}C)}$ (s)[b]	$T_{B,s}^{(^{13}C)}$ (s)[c]	φ[d]
Mg–HHRz + AMUPol[e]	~112	420 ± 160	118	2840	0.38
Mn–HHRz + AMUPol[e]	~112	160 ± 40	96	1954	0.53
Mn–HHRz[f]	~114	8 ± 1	130	3043	1.13
$^{13}C,^{15}N_2$-urea + $MnCl_2$[f]	~114	>4	215	5074	0.085

[a] Measured inside MAS stator. [b]Fast (short) component. [c]Slow (long) component. [d]Proportionality factor according to Eq. (3). [e]Measured at magnetic field optimized for cross effect DNP with nitroxides (9.40 T). [f]Measured at magnetic field optimized for ^{13}C solid effect DNP with Mn^{2+} (9.434 T)

spectrometer operating at 401.7 MHz ^1H frequency. The Bruker Ascent DNP magnet was centered at 9.40 T and contained a superconducting sweep coil with a range of ±70 mT. The sweep coil was energized so that a field of 9.434 mT was reached. After the optimum DNP enhancement was achieved the sweep unit was put into persistent mode. The NMR frequencies were roughly re-calibrated using a ^1H Bloch decay and further referenced on the RNA spectrum. 263.4 GHz microwaves were produced by a Bruker gyrotron operating at the maximum beam current of 115 mA. Experiments were performed at 114 K (mw on) or 105 K (mw off), read out via a thermocouple inside the MAS stator.

For all experiments radio frequency (rf) pulse powers were set to 100, 50, and 40 kHz for ^1H, ^{13}C, and ^{15}N, respectively; ^1H power was matched to ^{13}C or ^{15}N during Hartmann-Hahn CP. SPINAL64 at 100 kHz was used for broadband decoupling of ^1H. All one-dimensional spectra were measured after applying a pre-saturation pulse train and subsequent polarization delay; for the acquisition of build-up curves this delay was varied. The sample was contained within a 3.2 mm sapphire rotor (Bruker) and sealed with silicone soft plug and ZrO_2 drive cap. Magic-angle spinning with a spinning frequency of 10 kHz was used for all experiments except proton-driven spin diffusion (PDSD) correlation spectra where 10.8 kHz was utilized.

Results and discussion

EPR spectroscopy of the Mn–HHRz complex

The 180 GHz EPR spectrum of a frozen solution of the Mn^{2+} complex of HHRz (Mn–HHRz) is depicted in Fig. 2 and shows only minor differences to the hexaaquo complex (not shown). This is in agreement with previous comparisons at X- and Q-band frequencies (Morrissey et al. 2000). The occurrence of a significantly larger electric field gradient in the HHRz complex and thus resulting zero-field splitting (electron quadrupole interaction) in combination with slow tumbling of the biopolymer leads to a very broad EPR spectrum in liquid solution. This allows for

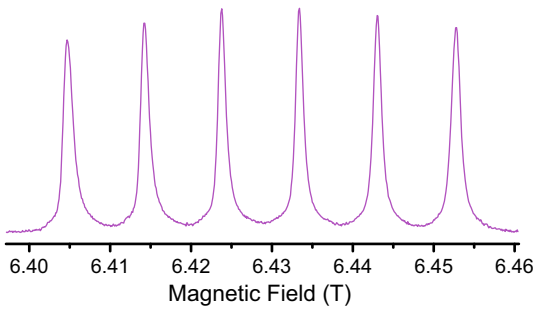

Fig. 2 180 GHz field-swept, electron spin echo detected EPR spectrum of Mn–HHRz in 60/40 (v/v) glycerol/water at 80 K

unambiguous and quantitative determination of "free" (i.e. not bound to HHRz) Mn^{2+} by titration. Using continuous-wave (cw) EPR spectroscopy at X-band frequency (9.4 GHz) we have confirmed binding of a single Mn^{2+} with a dissociation constant in agreement with the previously reported value of $K_D \approx 4$ μM (Horton et al. 1998; Schiemann et al. 2003) even at the relatively low NaCl concentration of 200 mM (Fig. S2). Because samples used for DNP-enhanced NMR spectroscopy are prepared with a large concentration of cryoprotecting glycerol we also verified quantitative binding of Mn^{2+} to HHRz in the same samples after recording of NMR spectra. We were unable to detect any unbound Mn^{2+} (see Fig. S3) and therefore estimate the ratio of "free" Mn^{2+} to overall added Mn^{2+} to be below 10 % which is in line with a dissociation constant in the low μM range.

By using these methods the error in estimated K_D is relatively large, and practically no conclusion can be drawn on the position and nature of the binding site. Nevertheless, these experiments confirm that the majority of HHRz is binding a single Mn^{2+}. This is the most important factor for the further analysis of direct, intra-complex DNP of ^{13}C as well as the investigation of paramagnetic interactions by Mn^{2+} on indirect ^1H DNP.

Direct DNP of Mn–HHRz using endogenous Mn^{2+}

Since typically commercial DNP spectrometers are optimized for ^1H cross effect DNP using bis-nitroxide

polarizing agents, it was required to shift the magnetic field to the ^{13}C solid effect matching condition of Mn^{2+} for the first demonstration employing the endogenous, paramagnetic metal center as polarizing agent for a biomolecule. The matching condition was estimated based on a simulated EPR spectrum using Easyspin (Stoll and Schweiger 2006) and spectral superposition of the electron–nuclear double and zero quantum transitions (Shimon et al. 2012). The procedure is described in more detail in the SI where we also show the simulation (Fig. S3). For exact matching of the external magnetic field we utilized a special DNP-dedicated NMR magnet (Bruker Ascent DNP) featuring a superconducting sweep coil. After sweeping the magnet to the estimated position the field was optimized in order to maximize the intensity of the detected ^{13}C spectrum evoked by Bloch-decay under mw irradiation. In Fig. 3 the obtained ^{13}C spectrum is shown with and without mw irradiation. An enhancement factor of $\varepsilon = 8$ is induced by intra-complex ^{13}C SE DNP by Mn^{2+}.

DNP of HHRz using AMUPol

In comparison, we also show spectra which have been obtained with a "conventional" DNP approach, that is by adding AMUPol as bis-nitroxide biradical polarizing agent and employing ^{1}H (indirect) DNP prior to cross polarization to ^{13}C or ^{15}N (CPMAS). A rather small biradical concentration of 5 mM was chosen in order to minimize potential signal quenching and/or broadening due to the nitroxide spins and to be able to observe effects induced by paramagnetic Mn^{2+}. The ^{1}H DNP enhancement is unexpectedly large with $\varepsilon = 240 \pm 10$ (Fig. 4) which significantly surpasses what has been observed on protein solutions—even with larger biradical concentrations—under otherwise similar conditions. Even though enhancement factors as large as 235 have been observed with AMUPol in the case of a simple proline solution (Sauvée et al. 2013), ε is usually reduced within a protein by a factor of 2–3; this loss of polarization can be recovered by complete deuteration of non-exchangeable hydrogens (Akbey et al. 2010). Also, in highly biologically relevant mixtures such as cell envelopes or even whole cells the enhancement factor drops significantly with increasing complexity of environment (Renault et al. 2012). Therefore, we attribute the large enhancement in RNA to the absence of side-chain dynamics and most profoundly methyl groups which provide for a dominant mechanism of ^{1}H longitudinal relaxation by reorientation under similar conditions in proteins or lipids (Glowinkowski et al. 1997; Gutsche et al. 2004; Nozirov et al. 2006).

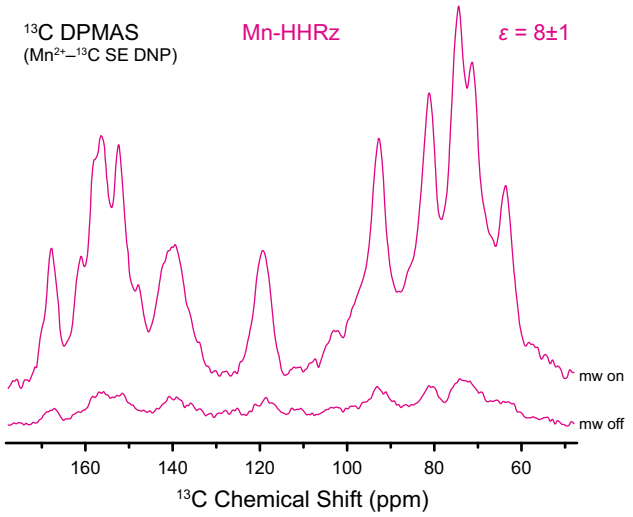

Fig. 3 ^{13}C DPMAS of Mn–HHRz, read-out via Bloch decay obtained by employing Mn^{2+} as only polarizing agent for SE at the matching field at 9.43 T; 0.75 ppm exponential line broadening was applied before Fourier transformation. On-spectra were obtained by co-adding 16 scans obtained with short (160 s) and 4 scans obtained with long (3276 s) polarization time, respectively. For the off-spectra we co-added 64 and 16 scans, respectively. Spectra are normalized with respect to number of scans. A complete compilation of individual direct-DNP enhanced spectra and their respective acquisition parameters is given in the SI (Fig. S5)

The large ^{1}H enhancement obtained with AMUPol seems to overshadow the relatively small enhancement factor of 8 induced by Mn^{2+} at first sight. Nonetheless, the demonstration of intra-complex DNP with an endogenously bound metal ion is an important step towards alternative approaches using internal polarizing agents. This becomes even clearer when this factor is compared to similar approaches where nitroxide labels covalently bound to lipids or proteins have been employed (Smith et al. 2015; Wylie et al. 2015). In these cases the observed enhancement factors were of the same magnitude.

We also prepared a diamagnetic RNA complex using Mg^{2+} as diamagnetic reference in order to assess the effects of paramagnetic Mn^{2+} on the NMR spectrum. The ^{1}H-DNP-enhanced ^{13}C and ^{15}N CPMAS spectra of this Mg–HHRz is shown in Fig. 4 in direct comparison with that of Mn–HHRz. Moderate reduction in signal amplitude is observed in the presence of Mn^{2+} for both ^{13}C and ^{15}N CPMAS. Nuclear resonance quenching depended mainly on the chemical environment: for ^{13}C directly bonded to ^{1}H we observed a $\sim$12–14 % reduction in peak height, while carbons not carrying hydrogen experienced a $\sim$20–30 % signal decrease; in the ^{15}N case the values converge to $\sim$16 and 19–22 % presumably due to longer required CP contact times. We tentatively attribute this signal reduction without apparent broadening to a $T_{1\rho}$-dominated paramagnetic relaxation mechanism during Hartmann-Hahn contact. Accelerated coherence decay and signal reduction by paramagnets in DNP samples has been observed in earlier studies (Corzilius et al. 2014; Lange et al. 2012;

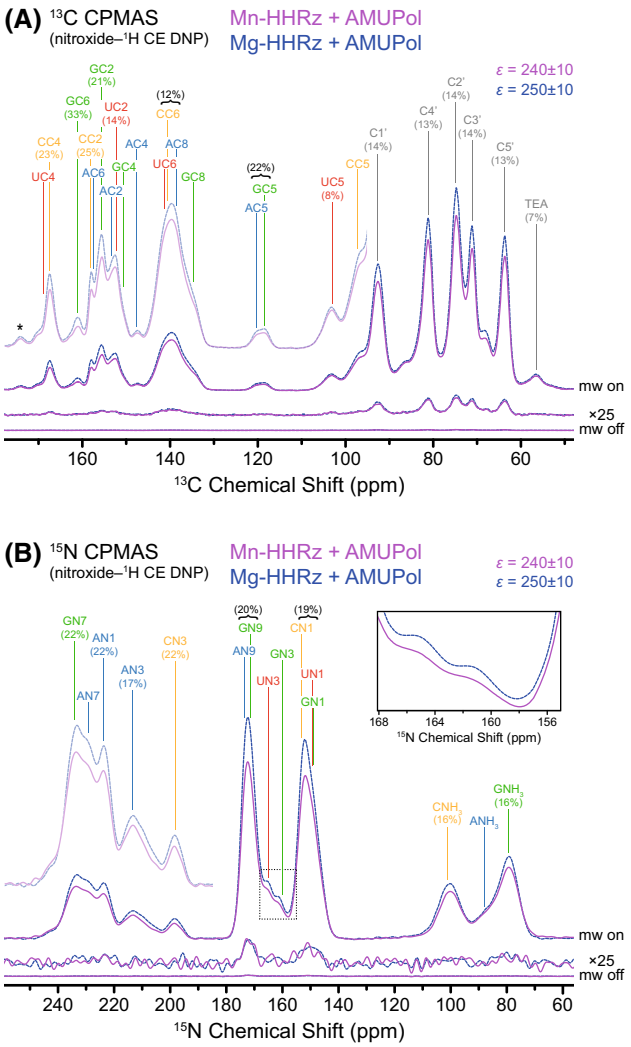

Fig. 4 DNP-enhanced ^{13}C (**a**) and ^{15}N (**b**) CPMAS spectra of Mn–HHRz (*solid magenta line*) and Mg–HHRz (*blue dashed line*) recorded with 16 scans and 64 scans, respectively; non-enhanced spectra (lower trace, 'mw off') are 512 scans in both cases. On- and off-spectra are normalized with respect to number of scans. Recycle delays were 9 and 10 s for the Mn- and the Mg–HHRz, respectively. The off-signal was also multiplied with a factor 25 (*middle trace*) for better visibility. Resonances have been assigned to nucleotide atoms based on two-dimensional spectra (see below); a MAS sideband from C5' is marked with an asterisk and a ^{13}C signal from TEA buffer in natural abundance is occurring around 57 ppm. Values in parentheses represent relative signal loss due to presence of Mn^{2+}; absolute intensities of spectra have been normalized by sample weight to correct for slightly different rotor filling. The lighter spectra are vertical magnifications with a factor 2.5 for better visibility of weaker signals. The *inset* shows the area marked by the *dotted box*

Rossini et al. 2012), but no difference has been observed between different nuclear environments in a biomolecule and a clear identification of the major mechanism to $T_{1\rho}$ relaxation has not been attempted. In order to investigate this effect further, CP build-up and/or $T_{1\rho}$ relaxation experiments on these HHRz samples are clearly of great interest and are planned in our lab.

The TEA signal at 57 ppm—which arises from homogeneously dispersed buffer molecules and therefore is expected to show the smallest effect due to Mn^{2+}—experienced only ~7 % signal reduction. Thus, the direct binding of Mn^{2+} to HHRz is reflected by a selective and significantly stronger quenching of RNA resonances.

Analysis of polarization build-up dynamics

The ^{1}H polarization build-up constant was determined by saturation recovery. The data could be fitted perfectly with a single exponential function and yielded $T_B^{^1H} = 7.1$ s. In the diamagnetic Mg–HHRz the time constant was slightly increased to 8.0 s (build-up curves are shown in the SI, Fig. S6). This is accompanied by a slightly increased ε of ~250 due to less efficient thermal contact of the ^{1}H spin bath to the lattice. The effects of Mn^{2+} on ^{1}H DNP are negligible which can be expected when extrapolating studies on paramagnetic effects to small paramagnet concentrations of <0.5 mM (Corzilius et al. 2014).

Direct polarization (DPMAS) read-out of ^{13}C using Bloch decay can potentially be a quantitative measure of polarization since it is not influenced by differences in ^{1}H environment. However, at cryogenic temperatures the longitudinal relaxation times of ^{13}C become prohibitively long for full recovery of longitudinal magnetization between scans. In fact, we observed large enhancements and a bi-exponential build-up behavior for both Mn- and Mg–HHRz (see Table 1 for details; a full overview of spectra and build-up curves is given in the SI, Figures S5 and S7). Using the fitting function

$$I(t) \propto \varphi\left[1 - \exp\left(-\frac{t}{T_{B,f}}\right)\right] + \left[1 - \exp\left(-\frac{t}{T_{B,s}}\right)\right], \qquad (3)$$

a fast (f) and a slow (s) build-up time constant have been determined which lie in the range of ~100 s and ~2000–3000 s, respectively, for all samples. We tentatively ascribe the fast and slow build-up components to a direct contact between ^{13}C and the electron spin(s) as well as relayed contact involving ^{13}C–^{13}C spin-diffusion through the ^{13}C depleted matrix (see details below). Furthermore, ^{13}C DPMAS spectra show visible broadening depending on the chosen pre-polarization delay (Fig. S5). This is caused by non-statistical weighting of resonances from nuclei in close proximity to the polarizing agent by fast longitudinal build-up and/or large DNP enhancements. The presence of Mn^{2+} again has a negligible impact on the observable spectrum. This might seem surprising, but can be explained by the relatively large concentration of AMUPol; at 5 mM each HHRz of about ~6 nm globular

diameter is surrounded statistically by ~4 AMUPol molecules (accordingly 8 nitroxide spins) within 1 nm distance. This could also explain the highly efficient direct ^{13}C DNP in the isotope-depleted matrix; however, unspecific interactions between RNA and AMUPol cannot be excluded at the present time. The single Mn^{2+} at the defined binding position on the other hand leaves many nuclei at a distance of 3 nm and larger. Nevertheless, we observed a significant reduction in ^{13}C enhancement from ~420 in Mg–HHRz to ~160 in Mn–HHRz, leaving us with the conclusion that ε is significantly reduced by more efficient nuclear spin–lattice relaxation induced by the paramagnetic metal ion.

Build-up time constants for direct Mn^{2+}–^{13}C SE DNP are similar to time constants measured for the Mg–HHRz samples including AMUPol and are significantly longer than those for Mn–HHRz including AMUPol (the latter two were measured under ^{13}C CE DNP). This seems natural because paramagnetic relaxation rates induced by Mn^{2+} and AMUPol are additive in first order. Interestingly, the relative contribution of the fast and slow build-up components are inverted compared to both AMUPol containing samples. We explain this by the occurrence of parallel, competing relaxation modes, namely a direct as well as a relayed polarization transfer pathway via ^{13}C–^{13}C spin diffusion. By depletion of the ^{13}C abundance in glycerol to 0.05 % not only a significant background signal is diminished but—more importantly—the ^{13}C–^{13}C spin-diffusion between RNA molecules is suppressed. Therefore, directly bound Mn^{2+} can transfer polarization more efficiently through the direct pathway while AMUPol—though a more efficient polarizing agent due to cross effect—relies on spin-diffusion through the matrix. In order to confirm this hypothesis we prepared a reference sample comprised of 225 mM ^{13}C,$^{15}N_2$-urea and 0.4 mM $MnCl_2$ dissolved in the same glycerol/water mixture. This sample provides concentrations of ^{13}C and Mn^{2+} which are equal to those in the Mn–HHRz solution; although both ^{13}C and Mn^{2+} are now homogeneously dispersed within the glassy matrix. In contrast to Mn–HHRz the bi-exponential polarization build-up features only a minor contribution of a fast component while the majority of spin polarization built up with a time constant of ~5000 s, as can be seen in Table 1 and Fig. 5. This confirms our initial assignment of polarization build-up modes due to the absence of any efficient direct DNP transfer pathway from Mn^{2+} to ^{13}C in combination with slow spin-diffusion through the diluted ^{13}C network. For DNP with AMUPol an intermediate situation is encountered: the large molar excess of biradicals leads to a high probability of sufficiently close RNA–nitroxide contacts and opens the direct polarization pathway, nevertheless, in significantly lower extend as compared to the endogenous polarizing agent.

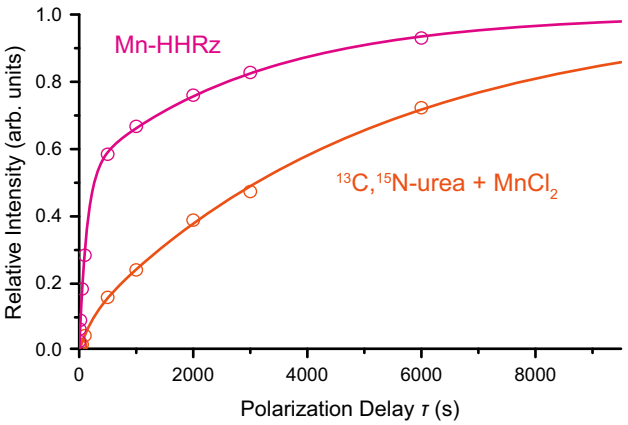

Fig. 5 Direct ^{13}C DNP build-up curves for 0.4 mM Mn–HHRz complex (*magenta*) and 0.4 mM $MnCl_2$ with 225 mM ^{13}C,$^{15}N_2$-urea (*orange*) both using Mn^{2+}–^{13}C SE DNP. *Curves* were obtained by pre-saturation of ^{13}C and following polarization delay of varying time τ and normalized to the extrapolated polarization at infinite time

Given the rather long polarization delays used for direct Mn^{2+}–^{13}C SE DNP (160 and 3276 s), enhanced magnetization can efficiently exchange throughout the uniformly labeled biomolecule by ^{13}C–^{13}C spin diffusion. Therefore, a site-selective enhancement cannot be expected. Nevertheless, we notice slight differences in relative peak intensities, most visible in the spectral area between 150 and 160 ppm. This might indicate selective resonance quenching/broadening and/or non-uniform enhancements of nuclei in the direct vicinity of Mn^{2+}. For further investigation of these sought-after effects, experiments using specifically isotope-labeled RNA are required in order to not only suppress equilibration of polarization by spin-diffusion but also to allow for unambiguous assignment of resonances to atomic sites in the large nucleic acid molecule.

Two-dimensional correlation spectroscopy

The large ^{1}H enhancements allowed us to obtain two-dimensional ^{13}C–^{13}C and ^{15}N–^{13}C correlation spectra with excellent signal-to-noise ratio in short time, as shown in Fig. 6. Since both techniques utilize ^{1}H magnetization with an initial ^{1}H–^{13}C or ^{1}H–^{15}N CP step, the enhancement factors measured by simple CP read-out also apply for the correlation spectra. Proton-driven spin diffusion (PDSD) was allowed for 100 ms mixing time for magnetization transfer over distances significantly longer than a C–C bond (Bloembergen 1949; Szeverenyi et al. 1982). In another experiment, transferred-echo double resonance (TEDOR) with a mixing time of 1.6 ms was utilized for recoupling of ^{15}N–^{13}C pairs in relatively close distance comparable to typically one to two bonds (Hing et al. 1992;

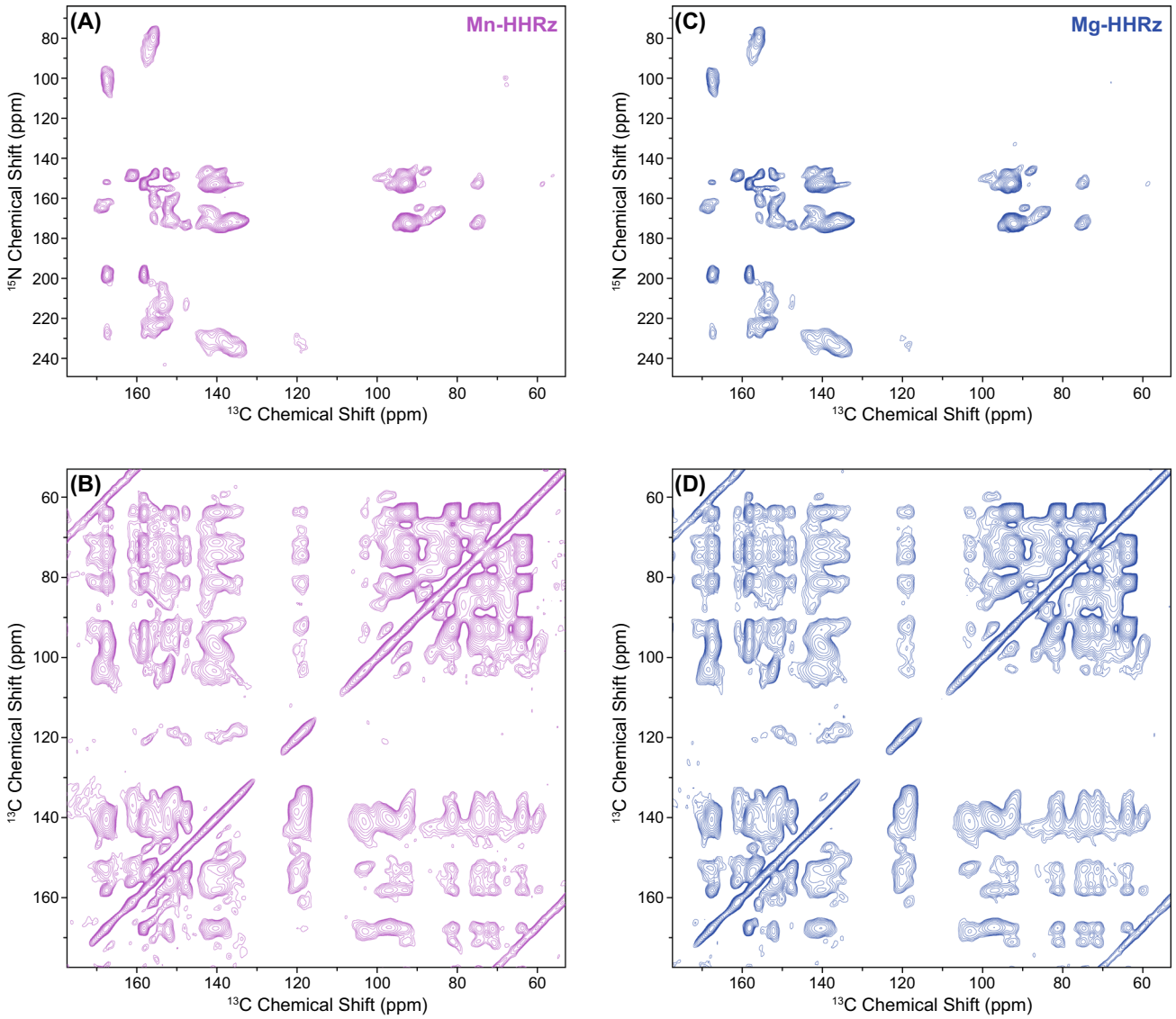

Fig. 6 DNP-enhanced ^{15}N–^{13}C TEDOR (**a**) and ^{13}C–^{13}C PDSD (**b**) correlation spectra of Mn–HHRz, and the respective TEDOR (**c**) and PDSD (**d**) spectra of Mg–HHRz. TEDOR spectra were recorded with 1.6 ms mixing time, 56 t_1 slices with 100 µs increment and 64 scans each (representing two 32-step phase cycles). Recycle delays of 8 and 9 s were used for Mn–HHRz and Mg–HHRz, respectively, resulting in 8 and 9 h acquisition time. A sine bell window function was applied in both dimensions and the spectra were Fourier-transformed after zero filling to 4096 × 1024 points. PDSD spectra were recorded with 100 ms mixing time, 128 t_1 slices with 44 µs increment and one 16-step phase cycle. A recycle delay of 9 s was used for both Mn–HHRz and Mg–HHRz, resulting in 5 h acquisition time. A sine bell window function was applied in both dimensions and the spectra were Fourier-transformed after zero filling to 4096 × 1024 points. All resonances above 170 ppm or below 62 ppm ^{13}C chemical shift are attributable to spinning sidebands

Jaroniec et al. 2002). Despite an overall intensity loss comparable to that observed in simple CP experiments, the effect of Mn^{2+} is minimal: only a very minor broadening can be observed in Mn–HHRz; additionally, several cross peaks show slightly larger relative intensity presumably due to more efficient recoupling by faster transverse relaxation during longitudinal mixing.

The combination of short range ^{15}N–^{13}C and long range ^{13}C–^{13}C correlations allowed us to assign a consistent set of resonances to the atoms in each nucleotide type (see SI, Tables S1 and S2, and Fig. S8). Every expected intra–nucleotide correlation has been clearly observed and assigned; additionally several inter–nucleotide resonances are visible and indicate close contacts due to base pairing or nucleotide stacking. Especially the resonances of cytidine-C5 and uridine-C5 show the largest number of unambiguous inter–nucleotide couplings due to their very large relative CP signal intensity caused by the directly bonded ^{1}H in combination with little spectral overlap. For the C6 atoms of the same nucleotides a similar situation is

expected, but mutual spectral overlap between cytidine-C6 and uridine-C6 and additional overlap with adenosine-C8 impedes unambiguous assignments. Also it is noteworthy that several nucleobase resonances feature a large chemical shift dispersion which is often correlated with a shift of a coupled resonance potentially allowing for the identification of structural elements given single-site resolution can be achieved by higher-dimensional correlation spectroscopy or selective isotope labeling.

In Fig. 7 we present slices taken out of the two-dimensional correlation spectra in order to demonstrate the impressive signal-to-noise ratio obtained by DNP. Clearly the enhanced signal intensity is sufficient to extend the space into three or even more dimensions for increased chemical shift dispersion selectivity and/or for peak assignment using more sophisticated strategies (Marchanka et al. 2013). Some broadening induced by Mn^{2+} seems to occur in the down-field shifted region above 140 ppm as is visible in the PDSD slice. This might arise from direct magnetic interactions between the electron spin of Mn^{2+} and the aromatic carbons of nucleobases close to the binding site. The large spectral overlap in the unselective one-dimensional CP experiment masks this broadening in Fig. 4.

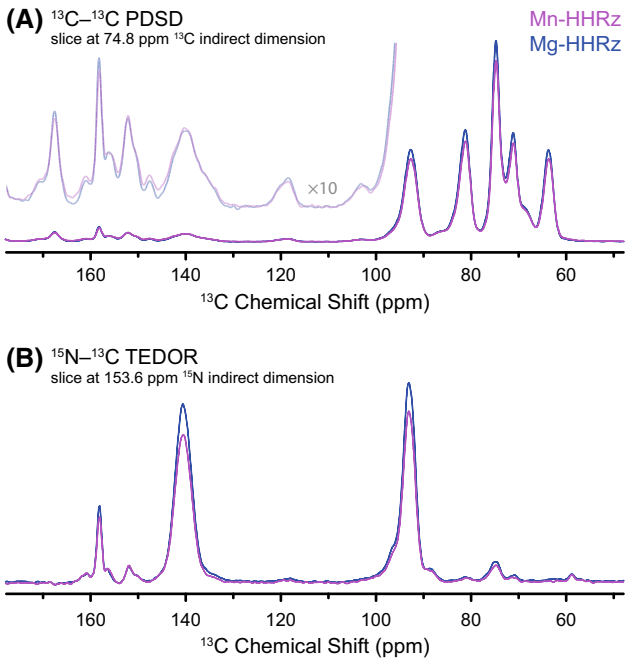

Fig. 7 One-dimensional slices of correlation spectra of Mn–HHRz and Mg–HHRz. **a** Slice taken out of PDSD (Fig. 6) at a ^{13}C chemical shift of 74.8 ppm corresponding to C2' resonance of all nucleotides. The *light lines* are a vertical magnification by a factor 10 for better visibility of the low-intensity aromatic regions. **b** Slice taken out of TEDOR (Fig. 6) at a ^{15}N chemical shift of 153.6 ppm corresponding to cytidine-N1 resonance. No apodization (window function) was applied in the direct dimension of both spectra to allow for demonstration of signal/noise ratio

Even though the intrinsically strong overlap of resonances in large nucleic acid molecules in the solid state often does not allow for assignment of individual nucleotides (Abramov and Goldbourt 2014), we can nevertheless identify several interesting, distinct spectral features not observed in solution NMR spectra of RNA. For example, we observe the occurrence of several ^{15}N correlation peaks to cytidine-C4 centered at a ^{13}C chemical shift of 167.3 ppm (see Fig. 8). A rather narrow but intense peak is found at a ^{15}N chemical shift of 198.2 ppm which we attribute to cytidine-N3 due to the sole coupling to cytidine-C2 at 158.2 ppm (besides C4). However, this resonance typically is reported to occur around 210 ppm with a narrow distribution. We found a broader resonance of smaller peak intensity at 227.3 ppm which is also coupled to cytidine-C2, -C4, and additionally to guanosine-C2 (although coupling to guanosine-C6 has not been observed). We tentatively attribute this to an alternative conformation of cytidine, which might be stabilized by Watson–Crick base pairing to guanosine. Fast exchange between these conformations in liquid state leads to coalescence of the resonances and occurrence of a single peak at the mean chemical shift of ~210 ppm. Please note that the simple analysis of peak intensities of the correlation spectra does not allow for the determination of conformational populations. A (tentatively assigned) third correlation resonance between cytidine-N3 and –C4 can be found at a ^{15}N chemical shift of 152.2 ppm. This significant upfield shift by ~50 ppm—together with observed coupling to ^{13}C resonances at 158.2 ppm (cytidine-C2) and ~134 ppm (guanosine-C8)—could be

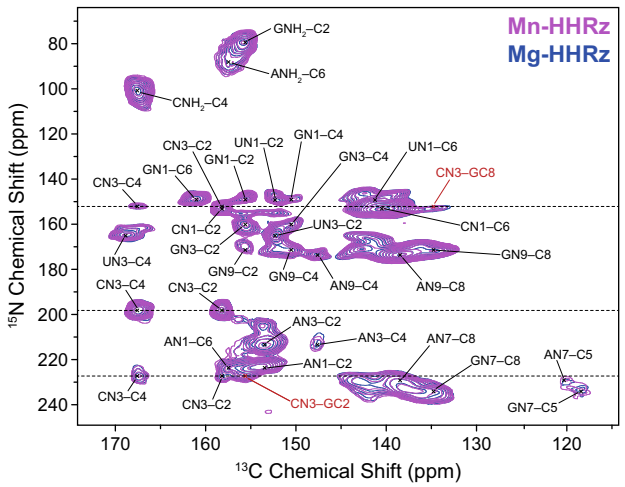

Fig. 8 Section of ^{15}N–^{13}C correlation spectrum showing heterogeneous splitting of cytidine-N3 into three resonances (marked with *dashed lines*). Resonances are labeled with nucleotide type (i.e. A, G, C, and U) and atom label according to Fig. S8. For inter-nucleotide contacts (*red*) both nucleotides are given in the label; for intra-nucleotide contacts (*black*) the nucleotide is given only as first character of the label

explained by protonation of cytidine-N3 and base pairing to guanosine in a Hoogsteen-type conformation. The occurrence of Hoogsteen-type base pairs in the tertiary structure of HHRz has been observed (Chi et al. 2008; Martick and Scott 2006). In order to vet this tentative conformational analysis further experiments are clearly required. Nevertheless, these preliminary findings clearly guide the way for future investigations.

Conclusion

In conclusion, uniformly isotope-labeled RNA can be efficiently polarized in a cryoprotecting frozen solution. The endogenously bound Mn^{2+} in HHRz can be used as polarizing agent for ^{13}C DNP of ribonucleic acid as we have shown in this first demonstration of direct, intra-complex DNP transfer in a biomolecule. Even though the enhancement factor is moderate and equilibration of enhanced polarization most probably occurs over the course of several tens or hundreds of seconds during build-up in uniformly ^{13}C-labeled biomolecules, the analysis of build-up dynamics in combination with potentially non-uniform enhancements in sparsely or selectively labeled samples might allow for the observation of site-selective DNP and may bear invaluable information for structural biology problems. Furthermore, with typical bis-nitroxide polarizing agents, ^{1}H enhancement factors of up to 250 have been observed which surpass those commonly observed in proteins due to the absence of fast-reorienting methyl groups. Furthermore, the presence of an endogenously bound paramagnetic Mn^{2+} ion only marginally influences the enhancement and linewidth as far as the analysis of overlapping resonances in the 59-mer allows. Analysis of two-dimensional ^{15}N–^{13}C and ^{13}C–^{13}C correlation spectra indicate the occurrence of multiple distinct conformations which would be interconverting in the liquid state but are trapped in the frozen solution. Therefore, MAS DNP in the cryogenic solid state allows for direct access of these otherwise "hidden" states as opposed to indirect detection methods in solution (Nikolova et al. 2011). During the preparation of this manuscript, Marchanka et al. have demonstrated nearly complete atomic site assignments of a small (26 nucleotides) RNA within a protein complex by MAS NMR (Marchanka et al. 2015). Extension of MAS NMR spectra to three or more spectral dimensions—not possible without the outstanding signal-to-noise ratio evoked by DNP (Marchanka et al. 2015)—would aid the development of efficient assignment protocols similar to those already available for proteins (Franks et al. 2007; Li et al. 2007; Pauli et al. 2001) and adapted for RNA structural biology by Marchanka et al. (Marchanka et al. 2013). This could establish DNP-enhanced MAS NMR as a valuable addition to the already existing toolbox for the structural biology of nucleic acids.

Additional information

Supporting Information. Native PAGE assay, dissociation constant determination, EPR confirmation of Mn^{2+} binding in DNP samples, Mn^{2+}–^{13}C SE simulation, full set of direct ^{13}C DNP spectra, build-up curves, and resonance assignment.

Acknowledgments This work was supported by the Deutsche Forschungsgemeinschaft (DFG) via Emmy Noether Grant CO802/2-1 issued to B.C. as well as DFG collaborative research center (Sonderforschungsbereich) 902, and by the Center for Biomolecular Magnetic Resonance (BMRZ). We thank J. Becker-Baldus and T. Gutmann for access to DNP spectrometers and technical assistance. Help from D. Akhmetzyanov during 180 GHz EPR experiments is gratefully acknowledged. We thank T. Prisner for proposing HHRz as the target system of this study, as well as H. Schwalbe and J. Wöhnert for helpful discussions. The sweepable MAS DNP NMR spectrometer was Granted to G. Buntkowsky (Darmstadt) via DFG Grant BU911/20-1.

Funding Deutsche Forschungsgemeinschaft (DFG) Grants CO802/2-1, SFB902, and BU911/20-1; Center for Biomolecular Magnetic Resonance (BMRZ).

Compliance with ethical standards

Conflict of interest The authors declare that they have no conflict of interest.

References

Abragam A, Proctor WG (1958) Une nouvelle méthode de polarisation dynamique des noyaux atomiques dans les solides. CR Hebd Acad Sci 246:2253–2256

Abramov G, Goldbourt A (2014) Nucleotide-type chemical shift assignment of the encapsulated 40 kbp dsDNA in intact bacteriophage T7 by MAS solid-state NMR. J Biomol NMR 59:219–230

Akbey Ü, Franks WT, Linden A, Lange S, Griffin RG, van Rossum BJ, Oschkinat H (2010) Dynamic nuclear polarization of deuterated proteins. Angew Chem Int Ed 49:7803–7806

Bassi GS, Murchie AI, Lilley DM (1996) The ion-induced folding of the hammerhead ribozyme: core sequence changes that perturb folding into the active conformation. RNA 2:756–768

Bayro MJ, Maly T, Birkett NR, MacPhee CE, Dobson CM, Griffin RG (2010) High-resolution MAS NMR analysis of PI3-SH3 amyloid fibrils: backbone conformation and implications for protofilament assembly and structure. Biochemistry 49:7474–7484

Becerra LR, Gerfen GJ, Temkin RJ, Singel DJ, Griffin RG (1993) Dynamic nuclear polarization with a cyclotron resonance maser at 5T. Phys Rev Lett 71:3561–3564

Beilstein K, Wittmann A, Grez M, Suess B (2015) Conditional control of mammalian gene expression by tetracycline-dependent hammerhead ribozymes. ACS Synth Biol 4:526–534

Bloembergen N (1949) On the interaction of nuclear spins in a crystalline lattice. Physica 15:386–426

Bothe JR, Nikolova EN, Eichhorn CD, Chugh J, Hansen AL, Al-Hashimi HM (2011) Characterizing RNA dynamics at atomic resolution using solution-state NMR spectroscopy. Nat Methods 8:919–931

Castellani F, van Rossum B, Diehl A, Schubert M, Rehbein K, Oschkinat H (2002) Structure of a protein determined by solid-state magic-angle-spinning NMR spectroscopy. Nature 420:98–102

Cherepanov AV, Glaubitz C, Schwalbe H (2010) High-resolution studies of uniformly ^{13}C,^{15}N-labeled RNA by solid-state NMR spectroscopy. Angew Chem Int Ed 49:4747–4750

Chi Y-I, Martick M, Lares M, Kim R, Scott WG, Kim S-H (2008) Capturing hammerhead ribozyme structures in action by modulating general base catalysis. PLoS Biol 6:2060–2068

Corzilius B, Smith AA, Barnes AB, Luchinat C, Bertini I, Griffin RG (2011) High-Field dynamic nuclear polarization with high-spin transition metal ions. J Am Chem Soc 133:5648–5651

Corzilius B, Smith AA, Griffin RG (2012) Solid Effect in magic angle spinning dynamic nuclear polarization. J Chem Phys 137:054201

Corzilius B, Andreas LB, Smith AA, Ni QZ, Griffin RG (2014) Paramagnet-induced signal quenching in MAS-DNP experiments on frozen homogeneous solutions. J Magn Reson 240:113–123

Dahm SC, Uhlenbeck OC (1991) Role of divalent metal ions in the hammerhead RNA cleavage reaction. Biochemistry 30:9464–9469

De la Peña M, Gago S, Flores R (2003) Peripheral regions of natural hammerhead ribozymes greatly increase their self-cleavage activity. EMBO J 22:5561–5570

Fernández-de-Alba C et al (2015) Matrix-free DNP-enhanced NMR spectroscopy of liposomes using a lipid-anchored biradical, chemistry. Eur J 21:4512–4517

Forster AC, Symons RH (1987) Self-cleavage of virusoid RNA is performed by the proposed 55-nucleotide active site. Cell 50:9–16

Franks WT, Kloepper K, Wylie B, Rienstra C (2007) Four-dimensional heteronuclear correlation experiments for chemical shift assignment of solid proteins. J Biomol NMR 39:107–131

Fürtig B, Richter C, Wöhnert J, Schwalbe H (2003) NMR spectroscopy of RNA. ChemBioChem 4:936–962

Fürtig B, Richter C, Schell P, Wenter P, Pitsch S, Schwalbe H (2008) NMR-spectroscopic characterisation of phosphodiester bond cleavage catalyzed by the minimal hammerhead ribozyme. RNA Biol 5:41–48

Glowinkowski S, Jurga S, Suchanski W, Szczesniak E (1997) Local and global dynamics in the glass-forming di-isobutyl phthalate as studied by ^{1}H NMR. Solid State Nucl Magn Reson 7:313–317

Gutsche P, Rinsdorf M, Zimmermann H, Schmitt H, Haeberlen U (2004) The shape and information content of high-field solid-state proton NMR spectra of methyl groups. Solid State Nucl Magn Reson 25:227–240

Hall DA, Maus DC, Gerfen GJ, Inati SJ, Becerra LR, Dahlquist FW, Griffin RG (1997) Polarization-enhanced NMR spectroscopy of biomolecules in frozen solution. Science 276:930–932

Hammann C, Norman DG, Lilley DMJ (2001) Dissection of the ion-induced folding of the hammerhead ribozyme using 19F NMR. Proc Natl Acad Sci U S A 98:5503–5508

Hing AW, Vega S, Schaefer J (1992) Transferred-echo double-resonance NMR. J Magn Reson 96:205–209

Horton TE, Clardy DR, DeRose VJ (1998) Electron paramagnetic resonance spectroscopic measurement of Mn^{2+} binding affinities to the hammerhead ribozyme and correlation with cleavage activity. Biochemistry 37:18094–18101

Hovav Y, Feintuch A, Vega S (2010) Theoretical aspects of dynamic nuclear polarization in the solid state—the solid effect. J Magn Reson 207:176–189

Hovav Y, Feintuch A, Vega S (2012) Theoretical aspects of dynamic nuclear polarization in the solid state—the cross effect. J Magn Reson 214:29–41

Hu KN (2011) Polarizing agents and mechanisms for high-field dynamic nuclear polarization of frozen dielectric solids. Solid State Nucl Magn Reson 40:31–41

Hu KN, Yu HH, Swager TM, Griffin RG (2004) Dynamic nuclear polarization with biradicals. J Am Chem Soc 126:10844–10845

Hu KN, Debelouchina GT, Smith AA, Griffin RG (2011) Quantum mechanical theory of dynamic nuclear polarization in solid dielectrics. J Chem Phys 134:19

Huang W, Bardaro MF Jr, Varani G, Drobny GP (2012) Preparation of RNA samples with narrow line widths for solid state NMR investigations. J Magn Reson 223:51–54

Hutchins CJ, Rathjen PD, Forster AC, Symons RH (1986) Self-cleavage of plus and minus RNA transcripts of avocado sunblotch viroid. Nucleic Acids Res 14:3627–3640

Jaroniec CP, Filip C, Griffin RG (2002) 3D TEDOR NMR experiments for the simultaneous measurement of multiple carbon-nitrogen distances in uniformly C-13, N-15-labeled solids. J Am Chem Soc 124:10728–10742

Jeffries CD (1957) Polarization of nuclei by resonance saturation in paramagnetic crystals. Phys Rev 106:164–165

Jeffries CD (1960) Dynamic orientation of nuclei by forbidden transitions in paramagnetic resonance. Phys Rev 117:1056–1069

Kessenikh AV, Lushchikov VI, Manenkov AA, Taran YV (1963) Proton polarization in irradiated polyethylenes. Sov Phys-Sol State 5:321–329

Khvorova A, Lescoute A, Westhof E, Jayasena SD (2003) Sequence elements outside the hammerhead ribozyme catalytic core enable intracellular activity. Nat Struct Mol Biol 10:708–712

Lange S, Linden AH, Akbey Ü, Franks WT, Loening NM, van Rossum B-J, Oschkinat H (2012) The effect of biradical concentration on the performance of DNP-MAS-NMR. J Magn Reson 216:209–212

Li Y, Berthold DA, Frericks HL, Gennis RB, Rienstra CM (2007) Partial ^{13}C and ^{15}N chemical-shift assignments of the disulfide-bond-forming enzyme DsbB by 3D magic-angle spinning NMR spectroscopy. ChemBioChem 8:434–442

Maly T, Miller AF, Griffin RG (2010) In situ high-field dynamic nuclear polarization-direct and indirect polarization of C-13 nuclei. ChemPhysChem 11:999–1001

Maly T, Cui D, Griffin RG, Miller A-F (2012) ^{1}H dynamic nuclear polarization based on an endogenous radical. J Phys Chem B 116:7055–7065

Marchanka A, Simon B, Carlomagno T (2013) A suite of solid-state NMR experiments for RNA intranucleotide resonance assignment in a 21 kDa protein–RNA complex. Angew Chem Int Ed 52:9996–10001

Marchanka A, Simon B, Althoff-Ospelt G, Carlomagno T (2015) RNA structure determination by solid-state NMR spectroscopy. Nat Commun 6:7024

Martick M, Scott WG (2006) Tertiary contacts distant from the active site prime a ribozyme for catalysis. Cell 126:309–320

Martick M, Lee T-S, York DM, Scott WG (2008) Solvent structure and hammerhead ribozyme catalysis. Chem Biol 15:332–342

Morrissey SR, Horton TE, Grant CV, Hoogstraten CG, Britt RD, DeRose VJ (1999) $Mn2^{+}$-nitrogen interactions in RNA probed by electron spin-echo envelope modulation spectroscopy: application to the hammerhead ribozyme. J Am Chem Soc 121:9215–9218

Morrissey SR, Horton TE, DeRose VJ (2000) Mn^{2+} sites in the hammerhead ribozyme investigated by EPR and continuous-wave Q-band ENDOR spectroscopies. J Am Chem Soc 122:3473–3481

Murray JB, Terwey DP, Maloney L, Karpeisky A, Usman N, Beigelman L, Scott WG (1998) The structural basis of hammerhead ribozyme self-cleavage. Cell 92:665–673

Ni QZ et al (2013) High frequency dynamic nuclear polarization. Acc Chem Res 46:1933–1941

Nikolova EN, Kim E, Wise AA, O'Brien PJ, Andricioaei I, Al-Hashimi HM (2011) Transient Hoogsteen base pairs in canonical duplex DNA. Nature 470:498–502

Nozirov F, Nazirov A, Jurga S, Fu R (2006) Molecular dynamics of poly(l-lactide) biopolymer studied by wide-line solid-state ^{1}H and ^{2}H NMR spectroscopy. Solid State Nucl Magn Reson 29:258–266

Osborne EM, Ward WL, Ruehle MZ, DeRose VJ (2009) The identity of the nucleophile substitution may influence metal interactions with the cleavage site of the minimal hammerhead ribozyme. Biochemistry 48:10654–10664

Overhauser AW (1953) Polarization of nuclei in metals. Phys Rev 92:411–415

Pauli J, Baldus M, van Rossum B, de Groot H, Oschkinat H (2001) Backbone and side-chain ^{13}C and ^{15}N signal assignments of the α-spectrin SH3 domain by magic angle spinning solid-state NMR at 17.6 Tesla. ChemBioChem 2:272–281

Pley HW, Flaherty KM, McKay DB (1994) Three-dimensional structure of a hammerhead ribozyme. Nature 372:68–74

Prody GA, Bakos JT, Buzayan JM, Schneider IR, Bruening G (1986) Autolytic processing of dimeric plant virus satellite RNA. Science 231:1577–1580

Renault M et al (2012) Solid-state NMR spectroscopy on cellular preparations enhanced by dynamic nuclear polarization. Angew Chem Int Ed 51:2998–3001

Rinnenthal J, Buck J, Ferner J, Wacker A, Fürtig B, Schwalbe H (2011) Mapping the landscape of RNA dynamics with NMR spectroscopy. Acc Chem Res 44:1292–1301

Rohrer M, Brügmann O, Kinzer B, Prisner TF (2001) High-field/high-frequency EPR spectrometer operating in pulsed and continuous-wave mode at 180 GHz. Appl Magn Reson 21:257–274

Rossini AJ et al (2012) One hundred fold overall sensitivity enhancements for Silicon-29 NMR spectroscopy of surfaces by dynamic nuclear polarization with CPMG acquisition. Chem Sci 3:108–115

Sauvée C, Rosay M, Casano G, Aussenac F, Weber RT, Ouari O, Tordo P (2013) Highly efficient, water-soluble polarizing agents for dynamic nuclear polarization at high frequency. Angew Chem Int Ed 52:10858–10861

Schiemann O, Fritscher J, Kisseleva N, Sigurdsson ST, Prisner TF (2003) Structural investigation of a high-affinity MnII binding site in the hammerhead ribozyme by EPR spectroscopy and DFT calculations. Effects of neomycin B on metal–ion binding. ChemBioChem 4:1057–1065

Scott WG, Finch JT, Klug A (1995) The crystal structure of an AII-RNA hammerhead ribozyme: a proposed mechanism for RNA catalytic cleavage. Cell 81:991–1002

Scott WG, Murray JB, Arnold JRP, Stoddard BL, Klug A (1996) Capturing the structure of a catalytic RNA intermediate: the hammerhead ribozyme. Science 274:2065–2069

Shimon D, Hovav Y, Feintuch A, Goldfarb D, Vega S (2012) Dynamic nuclear polarization in the solid state: a transition between the cross effect and the solid effect. Phys Chem Chem Phys 14:5729–5743

Smith AA, Corzilius B, Barnes AB, Maly T, Griffin RG (2012) Solid effect dynamic nuclear polarization and polarization pathways. J Chem Phys 136:015101

Smith AN, Caporini MA, Fanucci GE, Long JR (2015) A method for dynamic nuclear polarization enhancement of membrane proteins. Angew Chem Int Ed 54:1542–1546

Sripakdeevong P et al (2014) Structure determination of noncanonical RNA motifs guided by ^{1}H NMR chemical shifts. Nat Methods 11:413–416

Stoll S, Schweiger A (2006) EasySpin, a comprehensive software package for spectral simulation and analysis in EPR. J Magn Reson 178:42–55

Szeverenyi NM, Sullivan MJ, Maciel GE (1982) Observation of spin exchange by two-dimensional fourier transform ^{13}C cross polarization-magic-angle spinning. J Magn Reson 47:462–475

Wang S, Karbstein K, Peracchi A, Beigelman L, Herschlag D (1999) Identification of the hammerhead ribozyme metal ion binding site responsible for rescue of the deleterious effect of a cleavage site phosphorothioate. Biochemistry 38:14363–14378

Ward WL, DeRose VJ (2012) Ground-state coordination of a catalytic metal to the scissile phosphate of a tertiary-stabilized hammerhead ribozyme. RNA 18:16–23

Wasmer C, Lange A, Van Melckebeke H, Siemer AB, Riek R, Meier BH (2008) Amyloid fibrils of the HET-s(218-289) prion form a beta solenoid with a triangular hydrophobic core. Science 319:1523–1526

Wenckebach WT (2008) The solid effect. Appl Magn Reson 34:227–235

Wittmann A, Suess B (2011) Selection of tetracycline inducible self-cleaving ribozymes as synthetic devices for gene regulation in yeast. Mol BioSyst 7:2419–2427

Wylie BJ, Dzikovski BG, Pawsey S, Caporini M, Rosay M, Freed JH, McDermott AE (2015) Dynamic nuclear polarization of membrane proteins: covalently bound spin-labels at protein–protein interfaces. J Biomol NMR 61:361–367

Yen L et al (2004) Exogenous control of mammalian gene expression through modulation of RNA self-cleavage. Nature 431:471–476